

The SWELLS survey - V. A Salpeter stellar initial mass function in the bulges of massive spiral galaxies

Aaron A. Dutton^{1,2*} Tommaso Treu^{2†}, Brendon J. Brewer^{2,3}, Philip J. Marshall⁴,
M. W. Auger^{2,5}, Matteo Barnabè⁶, David C. Koo⁷, Adam S. Bolton⁸,
Leon V. E. Koopmans⁹

¹Max Planck Institute for Astronomy, Königstuhl 17, 69117, Heidelberg, Germany

²Dept. of Physics, University of California, Santa Barbara, CA 93106, USA

³Department of Statistics, The University of Auckland, Private Bag 92019, Auckland 1142, New Zealand

⁴Department of Physics, University of Oxford, Keble Road, Oxford, OX1 3RH, UK

⁵Institute of Astronomy, University of Cambridge, Madingley Rd, Cambridge, CB3 0HA, UK

⁶Kavli Institute for Particle Astrophysics and Cosmology, Stanford University, 452 Lomita Mall, Stanford, CA 94035, USA

⁷UCO/Lick Observatory, Department of Astronomy and Astrophysics, University of California, Santa Cruz, CA 95064, USA

⁸Department of Physics and Astronomy, University of Utah, Salt Lake City, UT 84112, USA

⁹Kapteyn Astronomical Institute, University of Groningen, P.O.Box 800, 9700 AV Groningen, The Netherlands

Accepted 2012 October 22. Received 2012 October 12; in original form 2012 June 19

ABSTRACT

Recent work has suggested that the stellar initial mass function (IMF) is not universal, but rather is correlated with galaxy stellar mass, stellar velocity dispersion, or morphological type. In this paper, we investigate variations of the IMF within individual galaxies. For this purpose, we use strong lensing and gas kinematics to measure independently the normalisation of the IMF of the bulge and disk components of a sample of 5 massive spiral galaxies with substantial bulge components taken from the SWELLS survey. We find that the stellar mass of the bulges are tightly constrained by the lensing and kinematic data. A comparison with masses based on stellar population synthesis models fitted to optical and near infrared photometry favors a Salpeter-like normalisation of the IMF. Conversely, the disk masses are less well constrained due to degeneracies with the dark matter halo, but are consistent with Milky Way type IMFs in agreement with previous studies. The disks are submaximal at 2.2 disk scale lengths, but due to the contribution of the bulges, the galaxies are baryon dominated at 2.2 disk scale lengths. Globally, our inferred IMF normalisation is consistent with that found for early-type galaxies of comparable stellar mass ($> 10^{11}M_{\odot}$). Our results suggest a non-universal IMF within the different components of spiral galaxies, adding to the well-known differences in stellar populations between disks and bulges.

Key words: dark matter — galaxies: bulges — galaxies: kinematics and dynamics — galaxies: spiral — gravitational lensing — stars: luminosity function, mass function

1 INTRODUCTION

The stellar initial mass function (IMF) is a fundamental quantity in many areas of astrophysics. From a theoretical standpoint, understanding the origin of the IMF from first principles is essential to develop a complete theory of star formation (e.g., McKee & Ostriker 2007). From a phenomenological standpoint, the IMF is a defining property of any stellar population, essential for computing quantities

such as stellar mass from observables, and for characterising their evolutionary history.

Traditionally, the main source of empirical evidence regarding the stellar IMF has been our own Milky Way, where individual stars can be identified and counted, first by Salpeter (1955). In the decades since then, only relatively small variations of the IMF have been found within our own Milky Way, despite enormous variations in the physical conditions within star-forming regions. These results have been generally interpreted as evidence that the IMF is more or less universal—i.e. it is insensitive to properties of the gas and dust in which stars form (e.g.,

* dutton@mpia.de

† Packard Research Fellow

Bastian et al. 2010). If indeed the IMF is universal, the kinematics of spiral (Bell & de Jong 2001) and elliptical galaxies (Cappellari et al. 2006), as well as lensing data (Brewer et al. 2012a, hereafter SWELLS-III) rule out IMFs like Salpeter’s implying relatively “heavy” mass-to-light ratios, in favour of “lighter” IMFs like that measured by Kroupa (2001) and Chabrier (2003).

However, recently a number of independent extragalactic studies have found significant deviations from the IMF as measured in the Milky Way. The observations are based on a variety of independent techniques, ranging from gravitational lensing (Treu et al. 2010, Auger et al. 2010, Spiniello et al. 2011, Brewer et al. 2012a), to stellar kinematics of elliptical galaxies (e.g., Dutton et al. 2012a,b; Cappellari et al. 2012a), and to spectral diagnostics of stellar populations (van Dokkum & Conroy 2010, 2011; Spiniello et al. 2012; Conroy & van Dokkum 2012).

Based on these observations, it appears that the IMF may depend on the stellar mass of the galaxy and hence on the cosmological time at which the stars formed, possibly reflecting the evolving physical conditions in the expanding universe. Or perhaps it could depend on the stellar velocity dispersion, reflecting the depth of the potential well. It is also possible that the IMF might depend on the morphological type of the galaxy, in the sense that early-type galaxies might have “heavier” IMFs than their spiral counterparts. However, the dependency of the distribution of morphological types on stellar mass (e.g., Blanton & Moustakas 2009), as well as the presence of two very distinct stellar populations in the bulge and disks of typical galaxies (e.g., Wyse, Gilmore, & Franx 1997) make it unclear whether the more important parameter is the overall stellar mass, or stellar velocity dispersion, or the morphological type.

In this paper we aim to gather some insight into the physical origin of the non-universality of the IMF by looking for variations *within* individual spiral galaxies. Is the normalisation of the IMF the same for bulge and disk, just varying with total stellar mass? Or is there one universal normalisation for disk-like stellar populations (presumably Chabrier-like) and a “heavier” (Salpeter-like) one for the older and more metal rich stellar populations found in massive bulges and spheroids? Clearly the two hypotheses are not mutually exclusive, as a combination of both could be at play.

Our strategy to constrain the IMF normalisation consists of comparing stellar masses derived from dynamics and strong lensing to those derived from stellar population synthesis (SPS) models. The main challenge of this approach – and of all other dynamical approaches – is that lensing and dynamics are sensitive to the total mass, and therefore one needs to disentangle the stellar mass from the non-baryonic dark matter. For disk-dominated galaxies it is well known that rotation curves can be fitted with a wide range of stellar mass-to-light ratios, from zero to maximum disk (e.g., van Albada & Sancisi 1986; Dutton et al. 2005), the so called disk-halo degeneracy (see however Amorisco & Bertin 2010). For bulge-dominated systems, the situation is similar in principle (the so-called bulge-halo degeneracy). However, if the stellar mass of the bulge dominates the inner parts of the gravitational potential, it is possible to get an actual measurement (rather than an upper limit), with only modest assumptions about the density profile of the dark mat-

ter halo, e.g., inspired by the results of cosmological numerical simulations (Treu & Koopmans 2002; Koopmans & Treu 2003; Treu et al. 2010; Auger et al. 2010; Cappellari et al. 2012a; see also Bertin et al. 1994, and references therein).

In order to study the IMF of the bulge and disk component we apply the lensing and dynamical technique to the sample of five massive ($V_{2.2} \sim 250 - 300 \text{ km s}^{-1}$, $M_{\text{SPS}}^{\text{Chab}} \sim 10^{11} M_{\odot}$) spiral lens galaxies in the SWELLS Survey (Treu et al. 2011, hereafter SWELLS-I) with significant bulges (bulge-to-disk ratio $\gtrsim 0.5$ assuming a universal IMF) and for which ionised gas kinematic data are available. SWELLS is a dedicated survey to the study of lensing spiral disk galaxies. Its main properties are summarized in Section 2. More details can be found in the paper by Treu et al. (2011). Thus, our mass models are constrained by the projected mass within the Einstein radius measured by strong gravitational lensing, by the rotation curve of the outer disk $\sim 1 - 3$ scale lengths from ionised gas kinematics, and the high resolution surface brightness profiles which are decomposed into a de Vaucouleurs bulge and an exponential disk. We derive stellar masses of the bulge and disk for a variety of assumptions about the structure of the dark matter halo, and compare the results with the estimates from stellar population synthesis models to infer the normalisation of the IMF independently for the two components.

This paper is organised as follows. In §2 we present the observational constraints. In §3 we present the mass models. In §4 we present of our main results. In §5 we discuss possible sources of systematic errors. In §6 we conclude with a brief summary. Throughout, we assume a flat Λ CDM cosmology with present day matter density, $\Omega_m = 0.3$, and Hubble parameter, $H_0 = 70 \text{ km s}^{-1} \text{ Mpc}^{-1}$.

2 SAMPLE SELECTION AND DATA

In this section we describe the sample selection and give a brief description of the data used in this paper. The reader is referred to papers SWELLS-I, SWELLS-II (Dutton et al. 2011b), SWELLS-III, and SWELLS-VI (Dutton et al., in preparation) for more details on the SWELLS selection and data.

2.1 Sample selection

As detailed in paper I, the parent SWELLS sample is selected from the Sloan Digital Sky Survey (SDSS) spectroscopic database based on the detection of emission lines at multiple redshifts within the $3''$ fiber and on having photometric axis ratio < 0.6 . Multiband Hubble Space Telescope imaging is used to confirm the lensing hypothesis. The sample of twenty confirmed lenses spans a broad range of bulge to total stellar mass ratio (from 0.1 to 0.9) for a fixed universal IMF, and a range in stellar mass of over one decade ($\sim 10^{10} M_{\odot}$ to $10^{11.5} M_{\odot}$; for a Chabrier IMF).

An important question is whether the SWELLS sample is representative of the overall population of spiral galaxies within the same ellipticity and stellar mass limits. Paper I shows that the size-stellar mass relation of the SWELLS sample is indistinguishable from that of a control sample of SDSS-selected galaxies using the same criteria. Paper VI will investigate the selection function in more detail using

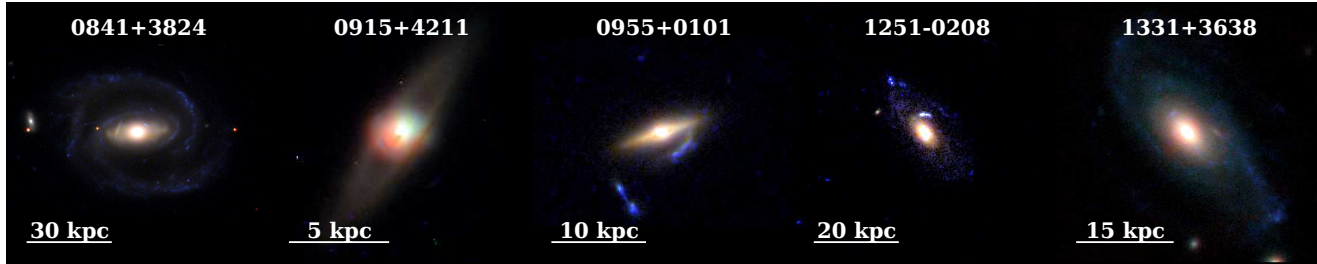


Figure 1. Postage stamp images of the galaxies analysed in this paper. The images are obtained from multicolour HST images as described in SWELLS-I and III.

Table 1. Basic properties of galaxies analyzed in this paper. All errors correspond to 1σ . Col. 1 lists the lens ID; Col. 2 the redshift of the deflector; Col.3 gives the velocity dispersion of the Singular Isothermal Ellipsoid (SIE) lens model from paper III; Cols. 4 and 5 give half-light sizes for the bulge (circularized) and disk (major axis) from papers I and III; Cols. 6, 7 and 8 give the stellar masses for the bulge, disk, and total, assuming a Chabrier (2003) IMF; Cols. 9 and 10 give the model (dust reddened) rest-frame V -band luminosities for the bulge and disk; Cols. 11 and 12 give the model (B-V) colors for the bulge and disk.

| ID | z_d | σ_{SIE} [km s $^{-1}$] | R_{bulge} [kpc] | R_{disk} [kpc] | $\log(M_{\text{SPS,b}}^{\text{Chab}})$ [M_{\odot}] | $\log(M_{\text{SPS,d}}^{\text{Chab}})$ [M_{\odot}] | $\log(M_{\text{SPS,t}}^{\text{Chab}})$ [M_{\odot}] | $\log(L_{V,b})$ [$L_{\odot,V}$] | $\log(L_{V,d})$ [$L_{\odot,V}$] | $(B-V)_b$ | $(B-V)_d$ |
|------------|-------|--|-----------------------------|----------------------------|---|---|---|--------------------------------------|--------------------------------------|-----------|-----------|
| (1) | (2) | (3) | (4) | (5) | (6) | (7) | (8) | (9) | (10) | (11) | (12) |
| J0841+3824 | 0.116 | 251.2 ± 4.4 | 2.42 | 23.43 | 11.05 ± 0.09 | 11.23 ± 0.09 | 11.45 ± 0.07 | 10.54 ± 0.04 | 10.84 ± 0.04 | 0.79 | 0.70 |
| J0915+4211 | 0.078 | 195.7 ± 2.2 | 1.56 | 4.15 | 10.60 ± 0.09 | 10.17 ± 0.09 | 10.74 ± 0.08 | 10.03 ± 0.05 | 9.73 ± 0.05 | 0.81 | 0.72 |
| J0955+0101 | 0.111 | 238.4 ± 7.3 | 1.62 | 3.72 | 10.63 ± 0.09 | 10.17 ± 0.09 | 10.76 ± 0.07 | 10.00 ± 0.04 | 9.73 ± 0.04 | 0.87 | 0.73 |
| J1251-0208 | 0.224 | 203.0 ± 2.6 | 1.68 | 12.01 | 10.68 ± 0.07 | 10.96 ± 0.07 | 11.14 ± 0.06 | 10.16 ± 0.04 | 10.68 ± 0.03 | 0.82 | 0.65 |
| J1331+3638 | 0.113 | 248.1 ± 4.4 | 2.86 | 12.46 | 10.89 ± 0.10 | 10.46 ± 0.10 | 11.03 ± 0.07 | 10.38 ± 0.04 | 10.34 ± 0.04 | 0.78 | 0.47 |

kinematic data to construct the Tully-Fisher, Faber Jackson and Fundamental Plane correlations.

The subsample analysed in this paper is selected from the SWELLS survey to include all the massive spiral galaxies with significant bulges for which gas-kinematic rotation curves are available. We require the stellar mass in the disk to be less than two times the stellar mass in the bulge, a criterion that is met by all but two of the lenses in our sample (we also exclude one system that has been shown to have a pseudo-bulge) although only 5 of these systems also have gas rotation curves available. A montage of our selected subsample of galaxies is shown in Figure 1. The sub-sample includes some (but not all) of the most massive SWELLS lenses. Quantitatively, the subsample spans a range in lensing velocity dispersion of 196-251 km s $^{-1}$, i.e. galaxies that are more massive than our own Milky Way, and spanning the 230 km s $^{-1}$ threshold below which paper III concluded that a global Salpeter IMF is on average ruled out by the data. Basic properties of the subsample analysed in this paper are given in Table 1.

2.2 Strong Lensing

Strong lensing models for our sample galaxies are presented in SWELLS-III. The parameter that is most directly constrained by strong lensing is the circularised Einstein radius b (Treu 2010, and references therein). This is defined to be the radius inside which the average surface density is equal to the critical density for strong lensing:

$$\frac{M_{\text{proj}}(b)}{\pi b^2} = \Sigma_{\text{crit}} \equiv \frac{c^2}{4\pi G} \frac{D_s}{D_{\text{ds}} D_d}. \quad (1)$$

Here D_s is the angular diameter distance from the observer to the source, D_d is the angular diameter distance from the observer to the deflector (i.e., the lens), and D_{ds} is the angular diameter distance from the deflector to the source. The critical density thus depends only on the distances to the lens and source, which are known for all our lens systems from the SDSS redshifts and our adopted cosmology.

For comparison to kinematics it is convenient to express the lensing results in terms of circular velocity or velocity dispersion, where $V_{\text{SIE}} = \sqrt{2}\sigma_{\text{SIE}}$. However, since the mass profiles are in general not isothermal, the conversion from projected mass into circular velocity at the Einstein radius is non trivial. For a total mass profile steeper than isothermal, which is the case for our galaxies, the circular velocity at the Einstein radius is larger than the nominal circular velocity of the singular isothermal ellipsoid (SIE) model.

Thus in our mass models in this paper we fit directly for b , rather than the mass projected within b (due to covariance between $M_{\text{proj}}(b)$ and b), or the derived circular velocity/velocity dispersion at the Einstein radius.

2.3 Gas kinematics

We obtained major axis long-slit spectra for all five galaxies with the Low Resolution Imaging Spectrograph (LRIS; Oke et al. 1995) on the Keck I 10-m telescope between November 2008 and April 2011. Typical exposure times were 60 minutes, with seeing conditions of FWHM ~ 1.0 arcsec. On the red side we used the 600/7500 line grating which gives a pixel scale of 1.26 Å px $^{-1}$. With a 1'' width slit the resulting spectral resolution is $\simeq 4.2$ Å, corresponding to velocity dispersion resolution of ~ 70 km s $^{-1}$ at the wavelength

of H α . We adopt spatial samplings of $\simeq 1''.1-1''.5$ (5-7 pixels) corresponding to ~ 1 data point per seeing FWHM.

We measured rotation curves by fitting Gaussians to one-dimensional spectra extracted along the slit. To improve centroiding accuracy we fitted the redshift of neighbouring emission lines simultaneously. The primary set of emission lines are H α 6563, [NII] 6583, 6548. The line flux ratios between the two [NII] lines were fixed at the expected values. The velocity dispersions of the line pairs were also imposed to be the same, but were allowed to be different than H α . The continuum was fitted with a 2nd order polynomial.

The observed rotation velocities are lowered from the true circular velocities by several effects. Firstly, there is a $\sin(i)$ term due to the inclination, i , of the galaxy with respect to the line of sight. Secondly, there is the (potential) position angle offset of the slit from the kinematic major axis. Thirdly there is beam smearing due to finite slit width and seeing. These effects are taken into account in our modelling. We create model velocity fields and extract flux weighted rotation velocities inside a $1''$ width slit, which has a position angle offset from the major axis. For this calculation we assume the line emitting gas traces the stellar disk. This assumption is the major source of systematic uncertainty in our models. To minimise the impact of the uncertainties in the beam smearing model we exclude from our fits the inner few arcseconds of the kinematic data. We also exclude data points where the rotation curve is strongly asymmetric (such as due to the bar in J0841+3824), or where the signal to noise is low (such as in inter spiral arm regions). We treat the disk inclination angle and slit position angle offsets as nuisance parameters, allowing them to vary over suitably chosen small ranges. We determine an initial guess for the inclination from the disk minor-to-major axis ratio q_d assuming $\cos(i) = \sqrt{(q_d^2 - q_0^2)/(1 - q_0^2)}$, where $q_0 \simeq 0.2$ (e.g., Hall et al. 2012) is the intrinsic disk thickness.

2.4 Bulge and disk structural parameters

The light profiles are decomposed into bulges and disks as described in papers SWELLS-I and III. The bulge light profile is assumed to follow a Sérsic $n = 4$ (de Vaucouleurs) profile, while the disk profile is assumed to be Sérsic $n = 1$ (exponential) profile. We note that 0841+3824 is a barred spiral galaxy. However, the bar is significantly fainter than the bulge (≈ 2 magnitudes) and therefore it can be considered negligible from a dynamical standpoint, within our desired level of precision, thus simplifying significantly the analysis.

2.5 Stellar Population Synthesis Masses

The photometry (typically in 4 bands, BVIK) is used to compute SPS masses using the method of Auger et al. (2009) together with Bruzual & Charlot (2003) SPS models. The SPS masses for the bulge and disk are computed using both Chabrier (2003) and Salpeter (1955) IMFs. We consider stellar populations described by 5 parameters: the total stellar mass M_{SPS} , the population age A , the exponential star formation burst timescale τ , the metallicity Z and the reddening due to dust, τ_V . We employ a uniform prior requiring $9 \leq \log_{10}(M_{\text{SPS}}/M_{\odot}) \leq 13$, the age is constrained

such that star formation began at some (uniformly likely) time between $1 \leq z \leq 5$, τ has an exponential prior with characteristic scale 1 Gyr, and we impose uniform priors on the logarithms of the metallicity and dust extinction such that $-4 \leq \log_{10} Z \leq -1.3$ and $-2 \leq \log_{10} \tau_V \leq 0.3$. We note that the priors are the same for the bulge and the disk components but are sufficiently conservative that they do not bias our results. The posterior PDF is sampled as described in Auger et al. (2009). The stellar mass estimates are the mean and standard deviation of the marginalised posterior PDF.

As discussed by several authors, especially for the old and mostly dust free populations found in massive bulges, the uncertainties in stellar mass inferred from colors are dominated by the IMF normalization (see, e.g., recent discussion by Newman et al. 2012, and references therein). The degeneracies between ages and metallicities typical of color-based inferences mostly cancel out when inferring stellar masses (Bell & de Jong 2001; Auger et al. 2009). Similarly, the effects of using different stellar population synthesis models are typically of order 0.05-0.1 dex for stellar populations not dominated by thermally pulsating AGB stars (e.g., Treu et al. 2010).

3 REFERENCE MASS MODEL

In this section we define our reference model, which we will use in Section 4 to interpret the data. This is a very general model and should be regarded as the one providing the definitive results of this paper. However, in order to test the robustness of our conclusions, in Section 5 we define and apply to our data a full battery of alternative models, including ones with adiabatic contraction and expansion, as well as models characterised by dark matter cores, by different implementations of the cosmologically motivated dark matter halos introduced here, and models without dark matter. As we will show, our conclusions are robust with respect to the choice of model. Therefore, the reader pressed for time can skip Section 5 and jump directly to the Summary after Section 4.

3.1 Overview

Our reference model is one with two baryonic components, a spherical bulge and a thin disk, and a generic dark matter halo, that includes as a subset standard profiles motivated by cosmological simulations. We refer to this model as the “free” dark matter model.

We model the bulge with a Hernquist (1990) profile, which is parametrised by its mass, M_{bulge} , and a half-mass radius, r_{bulge} . We model the disk with an exponential profile, which is parametrised by its mass, M_{disk} , and a half-mass radius r_{disk} . We model the dark matter halo with a generalised spherical Navarro, Frenk, White (1997, NFW) profile:

$$\rho(r) \propto (r/r_s)^{-\gamma} (1 + r/r_s)^{-3+\gamma}, \quad (2)$$

where γ is the inner slope (NFW corresponds to $\gamma = 1$), and r_s is the scale radius. The normalisation is determined by the virial velocity, V_{200} , which is defined at a radius, R_{200} , enclosing a mean density of 200 times the critical density

of the Universe at redshift zero. The relation between virial velocity, virial radius, and virial mass is thus given by

$$\frac{V_{200}}{[\text{km s}^{-1}]} = \frac{R_{200}}{[h^{-1}\text{kpc}]} = \left(G \frac{M_{200}}{[h^{-1}M_{\odot}]} \right)^{1/3}, \quad (3)$$

where $h = H_0/100 \text{ km s}^{-1}\text{Mpc}^{-1}$ and $G \approx 4.302 \times 10^{-6} \text{ km}^2\text{s}^{-2} \text{ kpc } M_{\odot}^{-1}$. This reference model thus has 7 parameters (4 for the baryons, 3 for the dark matter).

3.2 Constraints and priors

3.2.1 Baryons

The disk and bulge sizes are fixed to the values obtained from our photometric bulge-disk decompositions (from SWELLS I and III). This assumes negligible mass-to-light ratio gradients in the bulge and disk and leaves 2 free parameters, the masses of the bulge and the disk. For these we adopt uniform priors in $\log_{10}(M)$ over an interval bracketing the range of plausible values as inferred from SPS masses. In practice, we adopt a lower limit of half the SPS mass assuming a Chabrier IMF, and an upper limit of twice the SPS mass assuming a Salpeter IMF. For old stellar populations, this upper limit corresponds to a power-law IMF with slope $\simeq -3$.

3.2.2 Dark matter

For the inner slope of the dark matter density profile we adopt a uniform prior in the interval $0 \leq \gamma < 2$. The lower limit corresponds to a cored halo, while the upper limit corresponds to isothermal, which mimics strong halo contraction.

For the scale radius of the halo we adopt a prior based on the concentration mass relation of ΛCDM haloes from Macciò et al. (2008). The median relation is given by

$$\log_{10}(c) = 0.830 - 0.098 \log_{10} \left(\frac{M_{200}}{10^{12}h^{-1}M_{\odot}} \right). \quad (4)$$

The concentration, c , is defined to be the ratio between the virial radius and the radius where the slope of the density profile is -2 : $c = R_{200}/r_{-2}$. For an NFW halo $r_{-2} = r_s$, but for a generalised NFW halo $r_{-2} = r_s/(2 - \gamma)$. We adopt a Gaussian prior on $\log_{10}(c|M_{200})$ with standard deviation of 0.11 dex, which is the scatter in halo concentrations found in cosmological simulations (Macciò et al. 2008). This choice of prior is not critical to our results. Its main purpose is to introduce more freedom in the dark matter model than obtained by assuming a fixed scale radius (e.g., Treu et al. 2010; Cappellari et al. 2012a), and to ensure the scale radii are not unphysically large or small.

For the virial velocity of the dark matter halo we adopt a uniform prior in the interval: $V_{200}^{\min} \leq V_{200} \leq V_{200}^{\max} \text{ km s}^{-1}$. The lower limit to the virial velocity is obtained by assuming the baryon fraction (inside the virial radius) is equal to the cosmic baryon fraction, $f_{\text{bar}} = 0.16$, thus

$$V_{200}^{\min} = \left(\frac{GM_{\text{total}}}{f_{\text{bar}}/(1 - f_{\text{bar}})} \right)^{1/3} = \left(\frac{116.4}{\text{km s}^{-1}} \right) \left(\frac{M_{\text{total}}}{10^{11}M_{\odot}} \right)^{1/3}, \quad (5)$$

where the total stellar mass $M_{\text{total}} = M_{\text{bulge}} + M_{\text{disk}}$. Similarly, the upper limit V_{200}^{\max} , corresponds to a baryon-to-stars

conversion efficiency of 1%. This conservative limit is motivated by satellite kinematics, weak lensing and halo abundance matching, which find conversion efficiencies of $\gtrsim 2.5\%$ in massive galaxies (Dutton et al. 2010).

3.3 Mass model fitting

The model, parametrized by θ , is fitted to the kinematic and lensing data simultaneously using a Bayesian Markov Chain Monte Carlo approach similar to that used in previous SWELLS papers. Specifically we fit for the lensing Einstein radius, b , and the observed gas rotation curve $V_{\text{rot}}(r_i)$ using the standard likelihood function:

$$\mathcal{L}(\theta) = \exp \left\{ -\frac{[b - b^{\text{mod}}(\theta)]^2}{2\sigma_b^2} - \sum_i \frac{[V_{\text{rot}}(r_i) - V_{\text{rot}}^{\text{mod}}(\theta)]^2}{2\sigma_{V,i}^2} \right\}. \quad (6)$$

As described above, our model for the gas rotation curve takes into account beam smearing due to seeing and finite slit width.

4 RESULTS

The results presented in this section are based on models with the “free” dark matter halo described in Section 3. As discussed in § 5, none of our main results are sensitive to the functional form of the dark matter halo that we adopt.

The results of our fits to the rotation curves and lensing Einstein radii are shown in the right panels of Fig. 2. The black shaded region shows samples of acceptable models, which should be compared to the red and blue data points (which correspond to the receding and approaching sides of the rotation curve, respectively). The inset panels show the 1 and 2 σ constraints on the Einstein radius from strong lensing (SWELLS-III). The model Einstein radii are shown as histograms. The orange shaded regions show the 68% confidence regions on the total circular velocity. The magenta, blue and grey shaded regions show the decomposition into bulge, disk, and dark matter, respectively. Overall the models fit the data remarkably well and allow us to answer some specific questions.

4.1 Is the IMF universal within individual galaxies?

The posterior probability distribution functions (PDFs) for the bulge and disk masses are shown in the left panels of Fig. 2 next to the corresponding rotation curves. The marginalised constraints on the bulge, disk, and total stellar masses are given in Table 2 (for reference, the corresponding masses from SPS models are given in Table 1). In the reference “free” models, the disk stellar masses are somewhat loosely constrained due to the well-known disk-halo degeneracy (e.g., van Albada & Sancisi 1986). However, the bulge masses are well constrained because the inner part of the mass density profile is too steep to be described by the dark matter halo.

The grey circles in Fig. 2 correspond to a universal Chabrier IMF. Three of the five galaxies in our sample are inconsistent (at greater than 2 σ level) with a universal Chabrier IMF in *both* the bulge and disk. A heavier IMF is

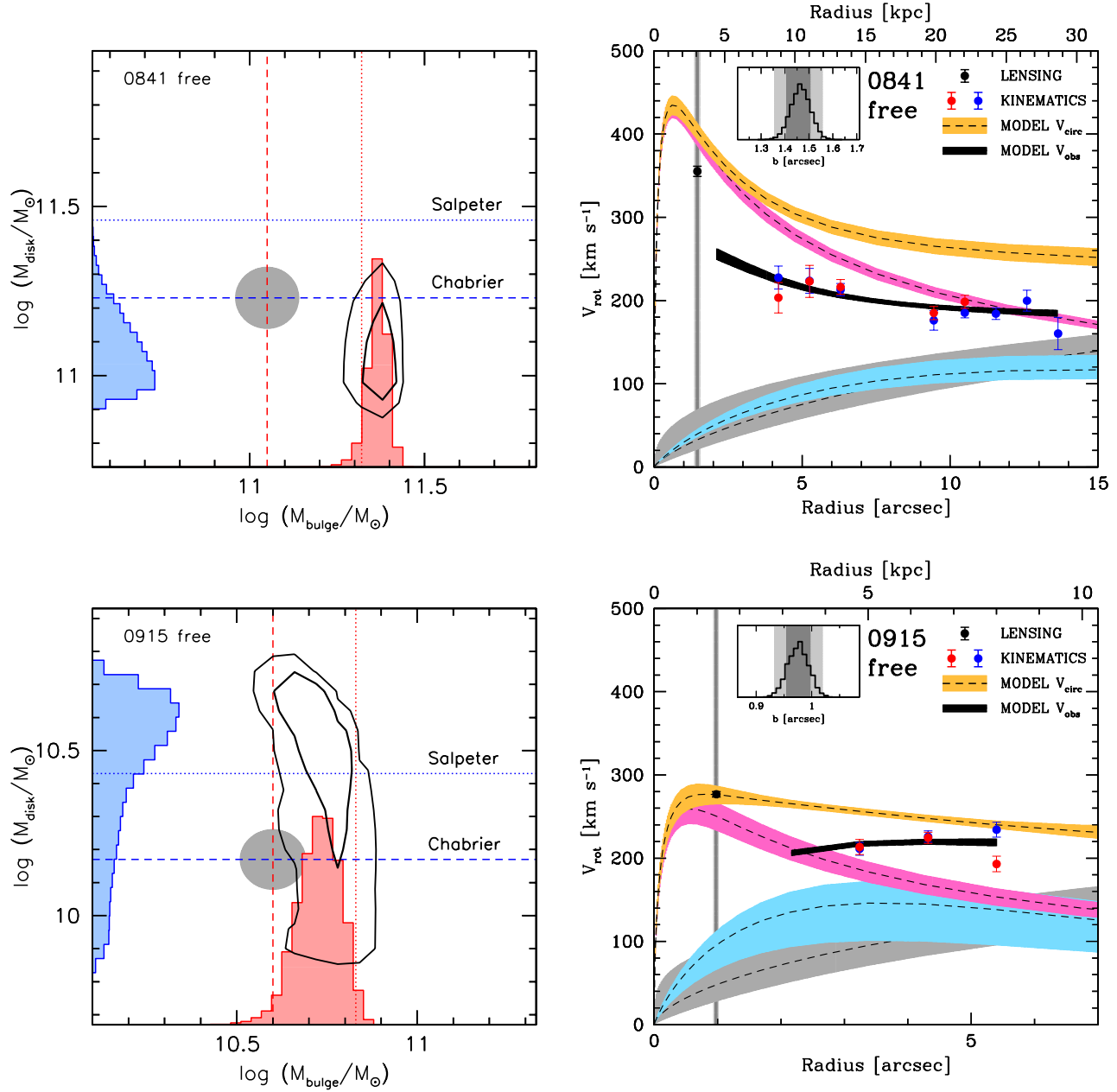


Figure 2. Mass model results for a free dark matter halo. *Left:* Joint constraints on bulge and disk masses. The contours enclose 68% and 95% of the probability. The red and blue histograms show the marginalised probability distributions for the bulge and disk masses, respectively. The dashed and dotted lines correspond to the median SPS masses assuming Chabrier and Salpeter IMFs, respectively. For reference, the grey ellipse shows the 1σ uncertainties on these SPS masses assuming a universal Chabrier IMF. *Right:* Data model comparison. The black shaded region shows the 68% confidence region of the “observed” model (including inclination and beam smearing effects). This should be compared to the red and blue points, which correspond to the observed rotation velocities from the receding and approaching sides of the galaxy, respectively. In the inset panels histograms show the distribution of model Einstein radii, while the shaded bands correspond to the 1 and 2σ constraints on the observed Einstein radii. These grey bands are repeated in the main panel. For reference the black point shows the circular velocity of the SIE model (note: this is not used in the fit). In the main panels, the orange shaded region shows the 68% constraint on the total circular velocity profile. The magenta, cyan, and grey shaded regions show the circular velocity profiles due to the bulge, disk, and dark matter halo, respectively. The bulge masses are well constrained due to the declining nature of the circular velocity curves, while the disk masses are less well constrained, due to degeneracies with the dark matter halo.

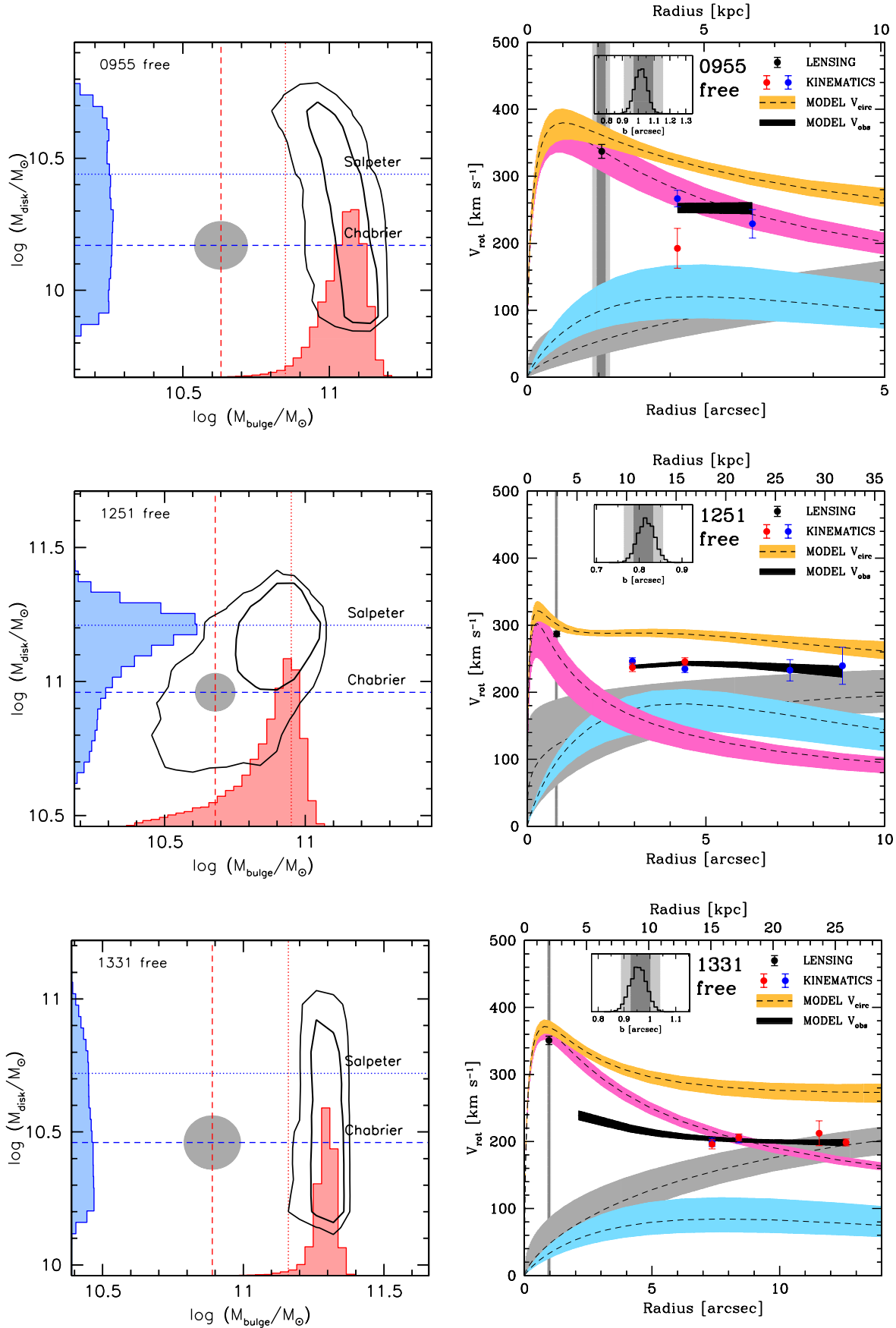


Figure 2. Continued

Table 2. Summary of stellar masses from fits to lensing and dynamics data with a free dark matter halo, and a comparison with SPS based masses. Cols 2,3, and 4 give the stellar masses (median together with 68% posterior probability) of the bulge, disk and total (bulge+disk); Cols 5,6, and 7 give the IMF mismatch parameter $\alpha \equiv M_{\text{LD}}/M_{\text{SPS}}^{\text{Chab}}$ (mean and standard deviation); Col 8 gives an upper limit to α within the Einstein radius using results directly from SWELLS-III.

| Name | $\log(M_{\text{LD,bulge}})$ | $\log(M_{\text{LD,disk}})$ | $\log(M_{\text{LD,total}})$ | $\log(\alpha_{\text{bulge}})$ | $\log(\alpha_{\text{disk}})$ | $\log(\alpha_{\text{total}})$ | $\log(\alpha_{\text{lens}})$ |
|------------|-----------------------------|----------------------------|-----------------------------|-------------------------------|------------------------------|-------------------------------|------------------------------|
| (1) | (2) | (3) | (4) | (5) | (6) | (7) | (8) |
| J0841+3824 | $11.37^{+0.02}_{-0.03}$ | $11.06^{+0.12}_{-0.09}$ | $11.54^{+0.05}_{-0.03}$ | 0.31 ± 0.10 | -0.15 ± 0.13 | 0.10 ± 0.08 | 0.29 ± 0.10 |
| J0915+4211 | $10.73^{+0.06}_{-0.06}$ | $10.50^{+0.14}_{-0.29}$ | $10.94^{+0.03}_{-0.07}$ | 0.13 ± 0.11 | 0.27 ± 0.24 | 0.18 ± 0.09 | 0.09 ± 0.10 |
| J0955+0101 | $11.06^{+0.06}_{-0.08}$ | $10.29^{+0.29}_{-0.27}$ | $11.14^{+0.03}_{-0.05}$ | 0.41 ± 0.12 | 0.12 ± 0.26 | 0.37 ± 0.09 | 0.41 ± 0.08 |
| J1251-0208 | $10.90^{+0.07}_{-0.16}$ | $11.16^{+0.10}_{-0.21}$ | $11.35^{+0.07}_{-0.18}$ | 0.18 ± 0.15 | 0.15 ± 0.17 | 0.17 ± 0.14 | 0.33 ± 0.07 |
| J1331+3638 | $11.29^{+0.03}_{-0.04}$ | $10.50^{+0.28}_{-0.23}$ | $11.37^{+0.05}_{-0.04}$ | 0.40 ± 0.11 | 0.06 ± 0.25 | 0.34 ± 0.09 | 0.42 ± 0.09 |
| Ensemble | | | | 0.29 ± 0.05 | -0.01 ± 0.12 | 0.24 ± 0.04 | |

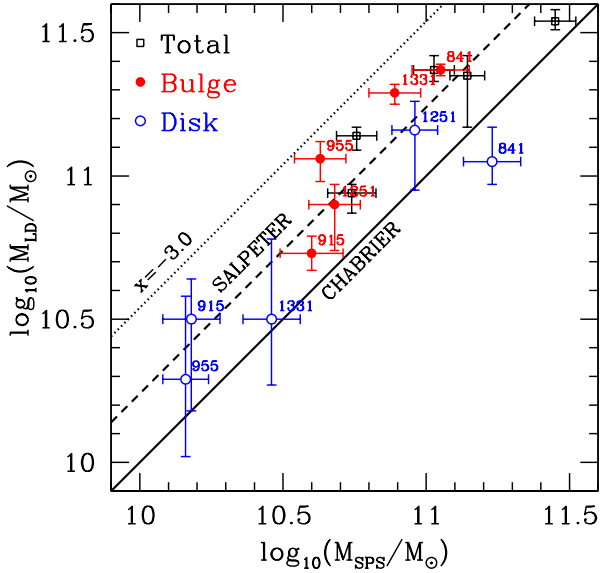


Figure 3. Comparison between bulge (red, filled circles), disk (blue, open circles) and total (black, squares) stellar masses from lensing plus dynamics, M_{LD} , with those from stellar population synthesis models assuming a Chabrier IMF, M_{SPS} . The error bars enclose 68% of the posterior probability. The disk masses of our five galaxies are consistent with a Chabrier IMF, but the bulge (and total) masses favour an IMF a factor of $\simeq 2$ heavier than Chabrier.

required for at least the bulge. Since Chabrier IMF seems to be in general preferred for starforming galaxy disks, our data indicate that the IMF may be non-universal *within galaxies*.

A comparison between the bulge and disk masses from our lensing plus dynamics analysis, M_{LD} , with those from SPS models, M_{SPS} , is shown in Fig. 3. For the disks, the LD masses are consistent with a Chabrier IMF, in agreement with previous studies of galactic disks (e.g., Bell & de Jong 2001; Bershady et al. 2011; Dutton et al. 2011a; Barnabè et al. 2012). However for the bulges, the LD masses are a factor of $\simeq 2$ higher than predicted by a Chabrier IMF and consistent with a Salpeter-like normalisation. This latter result is in agreement with studies of massive early-type galaxies (e.g., Auger et al.

2010; van Dokkum & Conroy 2010; Spiniello et al. 2012; Dutton et al. 2012b; Conroy & van Dokkum 2012). It is also interesting to note that the surface densities of the SWELLS bulges are comparable to the highest density ETGs in the local universe, which also favour IMFs with Salpeter-type normalisation (Dutton et al. 2012a).

Fig. 4 shows the PDFs for the “IMF mismatch parameter” Treu et al. (2010) $\alpha = M_{\text{LD}}/M_{\text{SPS}}$ quantifying the relation between between LD masses and SPS masses. Uncertainties on both measurements are taken into account when deriving the posterior distribution of α . The mean and standard deviation of the PDFs from Fig. 4 are given in Table 2. On average, the IMF of bulges is a factor of ~ 2 heavier than Chabrier ($\log \alpha_{\text{bulge}} = 0.29 \pm 0.05$), while the IMF of the disks is consistent with Chabrier ($\log \alpha_{\text{disk}} = -0.01 \pm 0.12$). We note that in 4 out of 5 galaxies the disk masses are also consistent with a Salpeter IMF. The total (bulge + disk) masses have $\log \alpha_{\text{total}} = 0.24 \pm 0.04$, which is consistent with a Salpeter-like normalisation of the IMF.

In SWELLS-III we concluded that a global IMF with α above the Salpeter value is ruled out (at 98% confidence) for galaxies with lensing velocity dispersions below 230 km s^{-1} . This might seem at odds with the conclusions of this paper. However, 3 out of the 5 galaxies studied here have velocity dispersion greater than 230 km s^{-1} (see Table 1). The galaxies with higher velocity dispersions all favor a bulge α values higher than the Salpeter value, while the galaxies with lower velocity dispersions favor bulge α values lower than the Salpeter value.

In addition, Table 2 gives the α parameter inside the Einstein radius calculated using results presented in SWELLS-III. Since these α are based on total masses, they are upper limits. Thus for consistency they should be larger than the α we derive in this paper. A direct comparison is complicated because the α ’s are measured in different apertures, but nevertheless, the α values for the bulges that we derive here are fully consistent with the upper limits from SWELLS-III.

4.2 Are disks sub-maximal?

The rotation curves of spiral galaxies have contributions from the stellar mass, gas mass, and dark matter. The relative contributions of each are difficult to estimate from rotation curve modelling due to well-known degen-

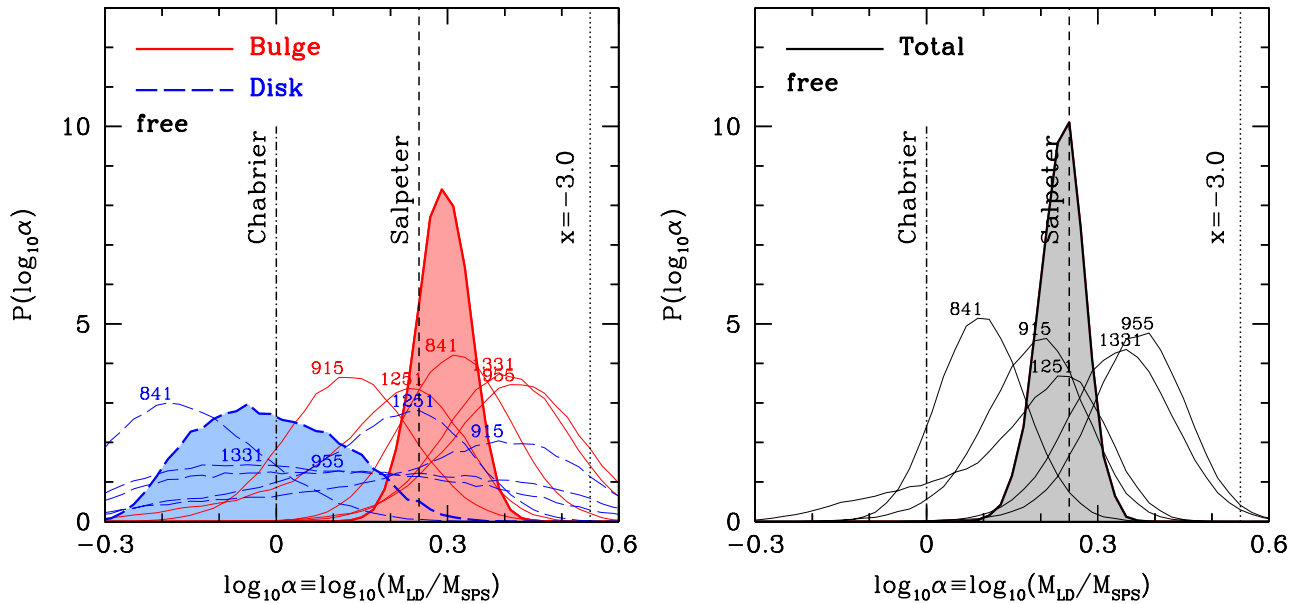


Figure 4. Posterior distributions for the IMF mismatch parameter relative to a Chabrier IMF, α . *Left:* for bulges (red, solid lines) and disks (blue, long dashed lines); *Right:* for total (bulge+disk) stellar mass. The bold histograms show the joint constraints on the mean α . Disks are consistent with a Chabrier IMF, while bulges require an IMF roughly twice as heavy as a Chabrier IMF. The overall normalisation is close to Salpeter.

eracies. This led to the maximum disk hypothesis (e.g., van Albada & Sancisi 1986) which proposes that the stellar disk makes the maximum possible contribution to the rotation curve.

According to the standard definition (Sackett 1997), a disk is maximal if its contribution to the circular velocity at 2.2 disk scale lengths is $0.75 < V_{\text{disk}}/V_{2.2} < 0.95$. This is shown as a blue shaded region in Fig. 5. The blue circles in Fig. 5 show that our five galaxies have $V_{\text{disk}}/V_{2.2} < 0.7$, and are thus sub-maximal. This is in broad agreement with results from the Disk Mass Project (solid and dashed lines in Fig. 5) which argued that all galaxy disks are sub-maximal (Bershady et al. 2011), in addition to earlier studies (e.g., Bottema 1993; Courteau & Rix 1999).

The galaxies in the Disk Mass Project are disk-dominated, so sub-maximal disks imply their galaxies are not baryon dominated inside 2.2 disk scale lengths (i.e., there is significant dark matter). However, in our galaxies there is a substantial bulge contribution (usually more than the disk) to $V_{2.2}$. The contribution of the stars (bulge plus disk) to $V_{2.2}$ is $\simeq 0.75$ to 0.95 (black points in Fig. 5), and thus these galaxies can be considered maximal in their total baryonic content at 2.2 disk scale lengths. (See also the results of the analysis of a disk galaxy lens including stellar kinematic constraints in SWELLS-IV, Barnabè et al. 2012.)

4.3 Are dark matter haloes cuspy?

The use of general dark matter haloes allows us to investigate the inner slope of the dark matter density profile, which is predicted by numerical simulations to be approximately unity, in the absence of baryons. Fig. 6 shows the PDFs of γ as inferred from our data. For individ-

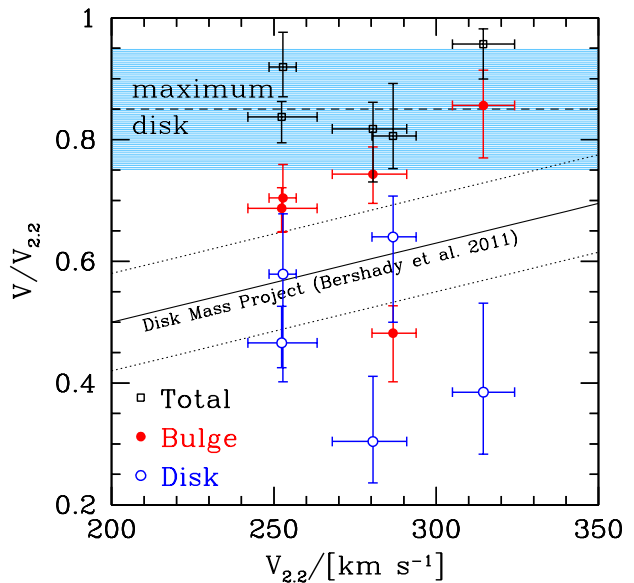


Figure 5. Contribution of disk, bulge and bulge+disk to circular velocity at 2.2 disk scale lengths. Disks are sub-maximal in agreement with the Disk Mass Project (Bershady et al. 2011), where the solid and dashed lines correspond to their best fit relation and scatter, respectively. However, the contribution of the disk plus bulge at 2.2 disk scale lengths is maximal, and thus our galaxies are baryon dominated within 2.2 disk scale lengths.

ual galaxies γ is only weakly constrained, reflecting the fact that the bulge stellar mass dominates in the inner regions. Taken as an ensemble, and assuming a univer-

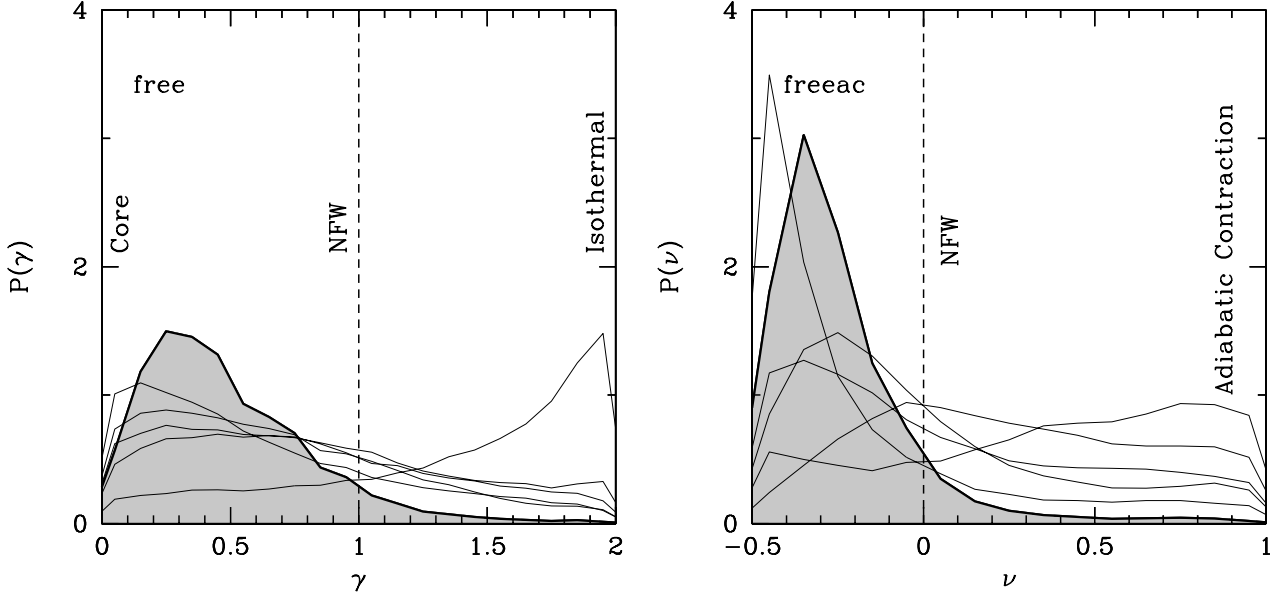


Figure 6. Posterior distributions for the central slope of the dark matter density profile, γ (left panel), and halo response parameter, ν (right panel). The bold histograms show the joint constraint on the mean. Haloes with $\gamma \gtrsim 1$ or halo contraction $\nu > 0$ are, on average, disfavoured.

sal value for γ , values larger than unity (i.e., NFW) are marginally disfavoured [$p(\gamma > 1) = 0.07$], consistent with what is found for early-type galaxies of comparable mass (Treu & Koopmans 2004; Dutton et al. 2012b), albeit there are counter-examples (Sonnenfeld et al. 2012; Grillo 2012), which may indicate that there is a broad scatter stemming perhaps from different formation histories.

At face value this result would imply a marginal conflict with the universal profiles predicted by cold dark matter only numerical simulations. However, since the central regions of these galaxies are baryon dominated, an accurate comparison depends crucially on how baryonic effects alter the underlying dark matter halos. Standard arguments suggest that baryonic cooling to form stars should steepen the overall mass density profile, thus causing the dark matter halo to steepen as well (Blumenthal et al. 1986; Gnedin et al. 2004). This would only exacerbate the tension between our observations and theoretical prediction. However, in practice other processes may occur that act to expand the halo, such as mass outflows due to stellar and/or active galactic nuclei (e.g., Read & Gilmore 2005; Duffy et al. 2010; Pontzen & Governato 2012) or dynamical friction between infalling galaxies and the dark matter halo (e.g., El-Zant et al. 2001; Johansson et al. 2009). Investigating this complex physics in detail goes beyond the scope of this paper, but it is interesting to notice that our data suggest that the net effect of baryonic physics appears to lead to real halos that are flatter or at most as flat as NFW, and not as cuspy as the standard contraction recipes would imply.

Table 3. Summary of priors on dark matter halo for our various mass models. $U(a, b)$ is a uniform prior with limits a , and b . $\delta(a)$ is a delta function prior at a .

| Model | γ | ν | r_s | V_{200} |
|--------|---------------|----------------|------------------------|-------------------------------------|
| free | $U(0.0, 2.0)$ | $\delta(0.0)$ | $r_s(V_{200})$ | $U(V_{200}^{\min}, V_{200}^{\max})$ |
| atlas | $U(0.0, 1.6)$ | $\delta(0.0)$ | $\delta(20\text{kpc})$ | $U(V_{200}^{\min}, V_{200}^{\max})$ |
| mfl | - | - | - | - |
| core | $\delta(0.0)$ | $\delta(0.0)$ | $r_s(V_{200})$ | $U(V_{200}^{\min}, V_{200}^{\max})$ |
| nfw | $\delta(1.0)$ | $\delta(0.0)$ | $r_s(V_{200})$ | $U(V_{200}^{\min}, V_{200}^{\max})$ |
| weakac | $\delta(1.0)$ | see text | $r_s(V_{200})$ | $U(V_{200}^{\min}, V_{200}^{\max})$ |
| ac | $\delta(1.0)$ | $\delta(1.0)$ | $r_s(V_{200})$ | $U(V_{200}^{\min}, V_{200}^{\max})$ |
| freeac | $\delta(1.0)$ | $U(-0.5, 1.0)$ | $r_s(V_{200})$ | $U(V_{200}^{\min}, V_{200}^{\max})$ |

5 TESTING SYSTEMATIC EFFECTS

In this section we discuss how our results depend on the functional form of the dark matter halo (§ 5.1), and we test potential systematic uncertainties arising from contamination of the lensing signal by mass along the line of sight (§ 5.2). In § 5.3 we discuss briefly the effects of neglecting cold gas in our lensing and dynamical analysis. We find that our conclusions are robust with respect to the choice of mass models and line of sight effects, and the inclusion of cold gas.

5.1 Alternative dark matter halo models

Our inferred dark matter profile is less cuspy than the NFW profile and one may be concerned that we have fitted away part of the central dark matter into our bulge component, thus leading to the preference for Salpeter-like IMFs over Chabrier. We therefore also consider a wide range of less flexible dark matter haloes, ranging from models with no dark matter or “mass-follows-light” (“mfl”), to cored dark matter

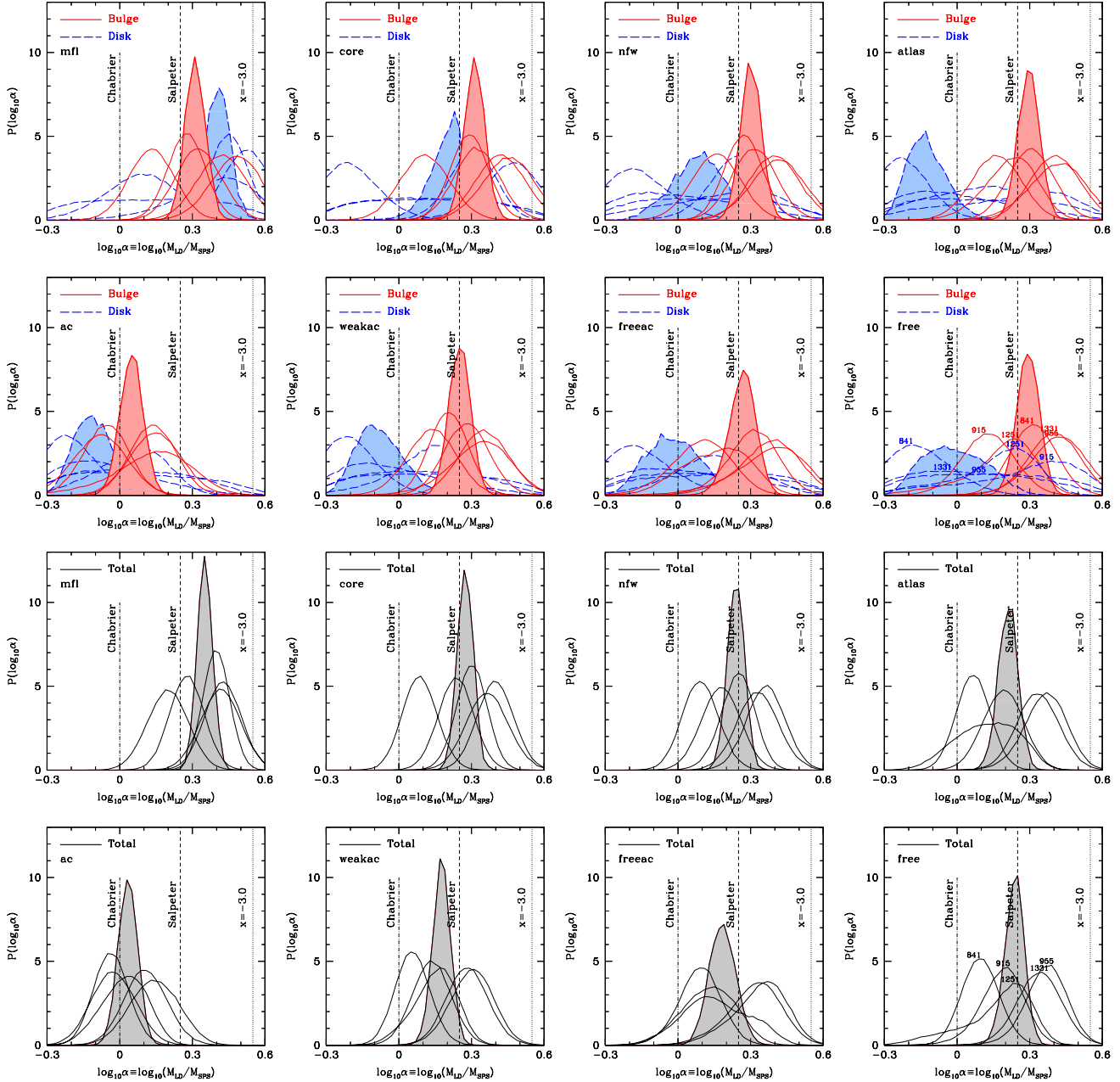


Figure 7. Posterior distributions for the IMF mismatch parameter relative to a Chabrier IMF, α , for eight different assumptions about the functional form of the dark matter halo: mfl — mass-follows-light (i.e., no dark matter halo); core — cored dark matter halo; nfw — Navarro, Frenk, White (1997) dark matter halo, constrained to follow the concentration–mass relation from Macciò et al. (2008) allowing for scatter; ac — adiabatically contracted nfw model; weakac — nfw model with weak halo contraction following Abadi et al. (2010); freeac — nfw model with free halo response ranging from adiabatic contraction to expansion; atlas — halo profile adopted by ATLAS3D (Cappellari et al. 2012a) which is a generalised NFW with fixed scale radius; free — generalised NFW halo with free inner slope (repeated from Fig. 4). *Upper:* α for bulges (red, solid lines) and disks (blue, long dashed lines); *Lower:* α for total (bulge+disk) stellar mass. The bold histograms show the joint constraints on the mean α . For all models except “ac” the bulges are consistent with a Salpeter IMF. For “ac” the bulges are consistent with a Chabrier IMF, but allowing the halo response to vary “freeac” generally finds better fits with weaker halo contraction or expansion.

haloes (“core”), to contracted NFW haloes (“ac”, “weakac”, and “freeac”). The most generic model adopted by the ATLAS3D team in their recent study (Cappellari et al. 2012a) is also included to facilitate comparisons between our works (“atlas”).

The contracted NFW halos are meant to represent the

response of the dark matter halo to galaxy formation. The simple model “ac” refers to the standard Blumenthal et al. (1986) formalism, the “weakac” model is the reduced contraction model of Abadi et al. (2010), while the “freeac” model is a generalisation. In the standard formalism the adiabatic invariant is $rM(r)$, where r is galactic radius and

$M(r)$ is the spherically enclosed mass within r . Thus

$$r_f/r_i = M_i(r_i)/M_f(r_f), \quad (7)$$

where r_i and r_f are the initial and final radii, respectively.

In order to explore the possibility of weaker halo contraction (e.g., Abadi et al. 2010) and even expansion, we also consider the generalised contraction formula from Dutton et al. (2007). If the standard contraction ratio from Eq. 7 is $\Gamma = (r_f/r_i)$, then the modified contraction ratio is given by Γ^ν . Standard adiabatic contraction (Blumenthal et al. 1986) corresponds to $\nu = 1$, the Gnedin et al. (2004) model can be approximated with $\nu \sim 0.8$, the Abadi et al. (2010) model can be approximated with $\nu \sim 0.4$, no contraction corresponds to $\nu = 0$, while expansion corresponds to $\nu < 0$.

Table 3 lists the dark halo priors for the eight models we consider here. We note that the models “core” and “nfw” are specific realisations of the model “free”, and the models “ac” and “nfw”, are specific realisation of the model “freeac”.

The posterior probability distribution functions for the IMF mismatch parameters of the bulge, disk, and total stellar mass for all models (our reference “free” model and alternatives) are given in Fig. 7. As expected, the disk masses are somewhat sensitive to the choice of dark matter halo. However, the bulge masses are remarkably insensitive to the dark matter halo model. All of the models, with the exception of adiabatically contracted NFW haloes (model “ac”), favour Salpeter-type IMFs for the bulges. The “ac” model is the only one that favours a Chabrier-type IMFs for the bulges. However, the fact that the “freeac” model contains the “ac” model allows us to perform a clean model selection procedure and quantify whether the models with Salpeter IMF or the “ac” model provide a better overall description of the data. Qualitatively, as can be seen from Fig. 6, the “freeac” model prefers values of the contraction index that disfavour the standard adiabatic contraction models. Quantitatively the comparison between the “freeac” model and the “ac” model is given by the evidence ratio (Sivia & Skilling 2006). The evidence of the “freeac” model is 35 times larger than that of the “ac” model, which corresponds to strong evidence that the first model is to be preferred according to standard criteria (Sivia & Skilling 2006). Similar considerations can be made for the IMF mismatch parameter α of the disks, although in general it is less well constrained than that of the bulge. All models with dark matter prefer disks that are Chabrier or lighter, except for the “nfw” and “core” models. Those are subsets of the “free” model and are disfavoured by the evidence ratios.

We thus conclude that *it is possible* to reconcile the data with a Chabrier IMF for bulges if one asserts that standard adiabatic contraction is the way dark matter halos respond to galaxy formation. However, cosmological simulations of galaxy formation often find much weaker contraction than predicted by the adiabatic contraction formalism (Johansson et al. 2009; Abadi et al. 2010; Tissera et al. 2010), or even expansion (Governato et al. 2010; Macciò et al. 2012) and thus we do not actually expect adiabatic contraction to occur in nature. Furthermore, under the more general assumption of ignorance about the effects of galaxy formation on the underlying dark matter halo, the data clearly prefer uncontracted or mildly expanded halos with a Salpeter IMF. This is true for a broad range of mod-

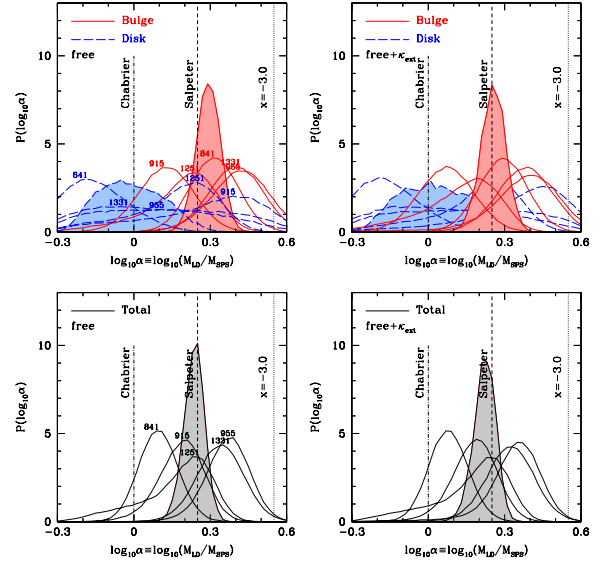


Figure 8. Effect of external convergence on the posterior distributions for the IMF mismatch parameter relative to a Chabrier IMF, α , for the “free” model. The model “free+ κ_{ext} ” (right panels) has the same dark matter halo as “free” (left panels, repeated from Fig. 4), except we have included 5% external convergence. The effect of external convergence is to lower α by a small amount.

els, including our “free” models, our “freeac” models, and the “atlas” models.

5.2 Line of sight effects

Another potential concern is whether excess mass along the line of sight could lead us to overestimate the mass associated with the main deflector and thus overestimate α . This is usually described in the lensing literature as external convergence (κ_{ext} , e.g., Treu et al. 2010; Suyu et al. 2010). The excess/deficit mass along the line of sight acts to first approximation as a sheet of mass at the redshift of the deflector, expressed in units of the critical density κ_{crit} , and cannot be measured with pure lensing arguments due to the well known mass-sheet degeneracy (Falco, Gorenstein, & Shapiro 1985). External convergence affects the lensing observable used in our analysis – the amount of mass within the Einstein Radius – in a very simple manner. The true mass will just be the observed mass obtained by assuming the line of sight has the average density of the universe, multiplied by $(1-\kappa_{\text{ext}})$, for small values of κ_{ext} .

At the relatively low redshift of the SWELLS and SLACS samples, external convergence is very small. Detailed analysis of the SLACS sample shows that the external convergence is typically a few percent (e.g., Treu et al. 2009; Guimarães & Sodr e 2011; Sonnenfeld et al. 2012). Thus, we expect that external convergence will change our results by a few percent at most. For completeness, we repeated all our inference assuming $\kappa_{\text{ext}} = 0.05$. As expected, α shifts down by a negligible amount (compare model “free” to “free+ κ_{ext} ” in Fig. 8) demonstrating that our inferences are robust with respect to line of sight effects.

5.3 Cold Gas

In principle the stellar masses derived from our lensing plus dynamics fits are upper limits, because we do not include cold gas in our mass models. For the stellar masses of our galaxies we expect cold gas fractions of $\sim 20 \pm 10\%$ (e.g., Dutton et al. 2011a), roughly equally split between atomic and molecular gas. Molecular gas generally traces the stars, and is typically less than $\sim 10\%$ of the stellar mass, assuming a Chabrier IMF (Saintonge et al. 2011), so the effect on our derived bulge stellar masses is expected to be less than 0.05 dex. The atomic gas typically has a larger scale length than the stellar disk, so we expect the atomic gas to subtract mass from the stellar disk and dark matter halo. In summary, we expect that including observations of cold gas in our mass models will not significantly reduce the derived stellar mass of the bulges.

6 SUMMARY

We have presented mass models of 5 massive galaxies selected from the SWELLS survey (Treu et al. 2011) to have bulges and disks of comparable stellar mass, as well as star forming disks. We combined masses from strong lensing with ionised gas kinematics at $\sim 1 - 3$ disk scale lengths to constrain the parameters of three component mass models consisting of a bulge, a disk and a generic dark matter halo. Our main results can be summarised as follows:

- The stellar masses of the bulges are well constrained by the lensing and kinematic data, independent of the inner density slope of the dark matter halo.
- The bulge masses inferred from the lensing and dynamical models, M_{LD} , are inconsistent with those obtained from the colours, M_{SPS} , assuming a Chabrier IMF, but in good agreement with those based on a Salpeter IMF. The average normalisation of the IMF of the bulges relative to that based on a Chabrier IMF, is given by the IMF mismatch parameter $\log_{10} \alpha_{bulge} \equiv \log_{10}(M_{LD,bulge}/M_{SPS,bulge}^{Chab}) = 0.29 \pm 0.05$
- The disk masses inferred from the lensing and dynamical models are only weakly constrained, due to degeneracies with the dark matter halo, but are consistent with a Chabrier-like IMF. The average IMF mismatch parameter is found to be $\log_{10} \alpha_{disk} = -0.01 \pm 0.12$.
- Disks are sub-maximal at 2.2 disk scale lengths (in agreement with the Disk Mass project, Bershady et al. 2011). However, baryons dominate the potential inside 2.2 disk scale lengths due to the strong bulge components. And thus sub-maximal disks do not imply galaxies are dark matter dominated inside 2.2 disk scale lengths.
- The data marginally disfavour an inner slope of the dark matter halo $\gamma > 1$ that would be expected for NFW halos contracted according to standard adiabatic contraction prescriptions. Equivalently, the data favour an uncontracted or marginally expanded NFW halo.

Our main new result is that IMF of bulges of spirals is “heavier” than Chabrier, and consistent with a Salpeter IMF. Since our data do not strongly constrain the IMF of the disks, there are two possible implications. Either the IMF varies *between* spiral galaxies (e.g., massive spiral galaxies have heavier IMFs than the Milky Way), or the

IMF varies *within* spiral galaxies (e.g., bulges have heavier IMFs than disks). Since all previous constraints on the masses of galactic disks seem to rule out Salpeter IMFs (e.g., Bell & de Jong 2001; Bershady et al. 2011; Dutton et al. 2011a; Martinsson 2011; Barnabè et al. 2012) we favor the latter hypothesis. Even though this result might seem surprising, it is well known that the stellar populations of bulges and disks differ in age and chemical composition. Thus, if the IMF reflects the physical conditions at the time of formation of the stellar populations, it is entirely possible that it could be different for the bulge and disk. Clearly, even though this is possible, the underlying physical reasons are at present unclear. Our hope is that this new piece of the puzzle will be a valuable clue for deciphering the mystery of the IMF and its variations across the universe.

To conclude we note that our results are consistent with previous work based on completely different techniques and samples when reframed in terms of a global IMF (as summarized by, e.g., Treu et al. 2010; Cappellari et al. 2012b). Furthermore our hypothesis of a different IMF for bulge and disk is consistent with the upper limits on total mass within the Einstein radius for the entire SWELLS and SLACS samples, presented in a companion paper (Brewer et al. 2012b, in preparation). Whereas SWELLS-III showed that the SWELLS and SLACS data are consistent with an IMF that changes as a function of galaxy stellar mass of stellar velocity dispersion, Brewer et al. (2012b) shows that a scenario where the IMF is Salpeter-like in the bulge and Chabrier-like in the disk is perfectly consistent with the lensing constraints.

ACKNOWLEDGEMENTS

AAD acknowledges financial support from the National Science Foundation Science and Technology Center CfAO, managed by UC Santa Cruz under cooperative agreement No. AST-9876783. AAD was partially supported by HST grants GO-12292, GO-11978, and GO-11202. TT acknowledges support from the NSF through CAREER award NSF-0642621, and from the Packard Foundation through a Packard Research Fellowship. PJM was given support by the Royal Society in the form of a research fellowship. MB acknowledges support from the Department of Energy contract DE-AC02-76SF00515. DCK acknowledges support from HST grant GO-11206.02-A, and NSF grant AST-0808133. LVEK acknowledges the support by an NWO-VIDI programme subsidy (programme number 639.042.505). This research is supported by NASA through Hubble Space Telescope programs GO-10587, GO-10886, GO-10174, 10494, 10798, 11202, 11978, 12292 and in part by the National Science Foundation under Grant No. PHY99-07949. and is based on observations made with the NASA/ESA Hubble Space Telescope and obtained at the Space Telescope Science Institute, which is operated by the Association of Universities for Research in Astronomy, Inc., under NASA contract NAS 5-26555, and at the W.M. Keck Observatory, which is operated as a scientific partnership among the California Institute of Technology, the University of California and the National Aeronautics and Space Administration. The Observatory was made possible by the generous financial support of the W.M. Keck Foundation. The authors

wish to recognize and acknowledge the very significant cultural role and reverence that the summit of Mauna Kea has always had within the indigenous Hawaiian community. We are most fortunate to have the opportunity to conduct observations from this mountain. Funding for the SDSS and SDSS-II was provided by the Alfred P. Sloan Foundation, the Participating Institutions, the National Science Foundation, the U.S. Department of Energy, the National Aeronautics and Space Administration, the Japanese Monbukagakusho, the Max Planck Society, and the Higher Education Funding Council for England. The SDSS was managed by the Astrophysical Research Consortium for the Participating Institutions. The SDSS Web Site is <http://www.sdss.org/>.

REFERENCES

- Abadi, M. G., Navarro, J. F., Fardal, M., Babul, A., & Steinmetz, M. 2010, *MNRAS*, 407, 435
- Amorisco, N. C., & Bertin, G. 2010, *A&A*, 519, A47
- Auger, M. W., Treu, T., Bolton, A. S., Gavazzi, R., Koopmans, L. V. E., Marshall, P. J., Bundy, K., & Moustakas, L. A. 2009, *ApJ*, 705, 1099
- Auger, M. W., Treu, T., Gavazzi, R., Bolton, A. S., Koopmans, L. V. E., & Marshall, P. J. 2010, *ApJL*, 721, L163
- Barnabè, M., et al. 2012, *MNRAS*, 423, 1073
- Bastian, N., Covey, K. R., & Meyer, M. R. 2010, *ARA&A*, 48, 339
- Bell, E. F., & de Jong, R. S. 2001, *ApJ*, 550, 212
- Bershady, M. A., Martinsson, T. P. K., Verheijen, M. A. W., Westfall, K. B., Andersen, D. R., & Swaters, R. A. 2011, *ApJL*, 739, L47
- Bertin, G., et al. 1994, *A&A*, 292, 381
- Blanton M. R., Moustakas J., 2009, *ARA&A*, 47, 159
- Blumenthal, G. R., Faber, S. M., Flores, R., & Primack, J. R. 1986, *ApJ*, 301, 27
- Bottema, R. 1993, *A&A*, 275, 16
- Brewer, B. J., et al. 2012a, *MNRAS*, 422, 3574
- Brewer, B. J., et al. 2012b, in prep
- Bruzual, G., & Charlot, S. 2003, *MNRAS*, 344, 1000
- Cappellari, M., et al. 2006, *MNRAS*, 366, 1126
- Cappellari, M., et al. 2012a, *Nature*, 484, 485
- Cappellari, M., et al., 2012b, *arXiv:1208.3523*
- Chabrier, G. 2003, *PASP*, 115, 763
- Conroy, C., & van Dokkum, P. 2012, *arXiv:1205.6473*
- Courteau, S., & Rix, H.-W. 1999, *ApJ*, 513, 561
- Duffy, A. R., Schaye, J., Kay, S. T., et al. 2010, *MNRAS*, 405, 2161
- Dutton, A. A., Courteau, S., de Jong, R., & Carignan, C. 2005, *ApJ*, 619, 218
- Dutton, A. A., van den Bosch, F. C., Dekel, A., & Courteau, S. 2007, *ApJ*, 654, 27
- Dutton, A. A., Conroy, C., van den Bosch, F. C., Prada, F., & More, S. 2010, *MNRAS*, 407, 2
- Dutton, A. A., Conroy, C., van den Bosch, F. C., et al. 2011a, *MNRAS*, 416, 322
- Dutton, A. A., et al. 2011b, *MNRAS*, 417, 1621
- Dutton, A. A., Mendel, J. T., & Simard, L. 2012a, *MNRAS*, 422, L33
- Dutton, A. A., Maccio, A.V., Mendel, J. T., & Simard, L. 2012b, *arXiv:1204.2825*
- El-Zant, A., Shlosman, I., & Hoffman, Y. 2001, *ApJ*, 560, 636
- Falco E. E., Gorenstein M. V., Shapiro I. I., 1985, *ApJ*, 289, L1
- Gnedin, O. Y., Kravtsov, A. V., Klypin, A. A., & Nagai, D. 2004, *ApJ*, 616, 16
- Governato, F., Brook, C., Mayer, L., et al. 2010, *Nature*, 463, 203
- Grillo C., 2012, *ApJ*, 747, L15
- Guimarães, A. C. C., & Sodr , L., Jr. 2011, *ApJ*, 728, 33
- Hall, M., Courteau, S., Dutton, A. A., McDonald, M., & Zhu, Y. 2012, *MNRAS*, 425, 2741
- Hernquist, L. 1990, *ApJ*, 356, 359
- Johansson, P. H., Naab, T., & Ostriker, J. P. 2009, *ApJL*, 697, L38
- Koopmans, L. V. E., & Treu, T. 2003, *ApJ*, 583, 606
- Kroupa, P. 2001, *MNRAS*, 322, 231
- Macci , A. V., Dutton, A. A., & van den Bosch, F. C. 2008, *MNRAS*, 391, 1940
- Macci , A. V., Stinson, G., Brook, C. B., et al. 2012, *ApJL*, 744, L9
- Martinsson, T. P. K. 2011, PhD thesis, University of Groningen
- McKee, C. F., & Ostriker, E. C. 2007, *ARA&A*, 45, 565
- Navarro, J. F., Frenk, C. S., & White, S. D. M. 1997, *ApJ*, 490, 493
- Newman A. B., Treu T., Ellis R. S., Sand D. J., 2012, *arXiv*, *arXiv:1209.1392*
- Oke, J. B., Cohen, J. G., Carr, M., et al. 1995, *PASP*, 107, 375
- Pontzen, A., & Governato, F. 2012, *MNRAS*, 421, 3464
- Read, J. I., & Gilmore, G. 2005, *MNRAS*, 356, 107
- Sackett, P. D. 1997, *ApJ*, 483, 103
- Saintonge, A., Kauffmann, G., Kramer, C., et al. 2011, *MNRAS*, 415, 32
- Salpeter, E. E. 1955, *ApJ*, 121, 161
- Sivia, D. S., & Skilling, J., 2006, *Data Analysis: A Bayesian Tutorial*, (2nd ed.; Oxford, Oxford University Press)
- Sonnenfeld A., Treu T., Gavazzi R., Marshall P. J., Auger M. W., Suyu S. H., Koopmans L. V. E., Bolton A. S., 2012, *ApJ*, 752, 163
- Spiniello, C., Koopmans, L. V. E., Trager, S. C., Czoske, O., & Treu, T. 2011, *MNRAS*, 417, 3000
- Spiniello, C., Trager, S. C., Koopmans, L. V. E., & Chen, Y. 2012, *ApJL*, 753, L32
- Suyu, S. H., Marshall, P. J., Auger, M. W., et al. 2010, *ApJ*, 711, 201
- Tissera, P. B., White, S. D. M., Pedrosa, S., & Scannapieco, C. 2010, *MNRAS*, 406, 922
- Treu, T., Gavazzi, R., Gorecki, A., et al. 2009, *ApJ*, 690, 670
- Treu, T., Auger, M. W., Koopmans, L. V. E., Gavazzi, R., Marshall, P. J., & Bolton, A. S. 2010, *ApJ*, 709, 1195
- Treu, T. 2010, *ARA&A*, 48, 87
- Treu, T., Dutton, A. A., Auger, M. W., Marshall, P. J., Bolton, A. S., Brewer, B. J., Koo, D. C., & Koopmans, L. V. E. 2011, *MNRAS*, 417, 1601
- Treu, T., & Koopmans, L. V. E. 2002, *ApJ*, 575, 87
- Treu, T., & Koopmans, L. V. E. 2004, *ApJ*, 611, 739
- van Albada, T. S., & Sancisi, R. 1986, *Royal Society of London Philosophical Transactions Series A*, 320, 447
- van Dokkum, P. G., & Conroy, C. 2010, *Nature*, 468, 940

van Dokkum, P. G., & Conroy, C. 2011, ApJL, 735, L13
Wyse R. F. G., Gilmore G., Franx M., 1997, ARA&A, 35,
637

This paper has been typeset from a \TeX / \LaTeX file prepared
by the author.